Available online at www.sciencedirect.com
SCIENCE DIRECT®
Journal of Magnetic Resonance 174 (2005) 116–124
JMR Journal of Magnetic Resonance
www.elsevier.com/locate/jmr

Passive shimming of the fringe field of a superconducting magnet for ultra-low field hyperpolarized noble gas MRI

Juan Parra-Robles [a,b,*], Albert R. Cross [a,c], Giles E. Santyr [a,b]

[a] Department of Physics, Carleton University, Ottawa, ON, Canada K1S 5B6
[b] Imaging Research Laboratories, Robarts Research Institute, London, ON, Canada N6A 5K8
[c] Department of Physics, University of Lethbridge, Lethbridge, AB, Canada T1K 3R4

Received 5 November 2004; revised 20 January 2005

Abstract

Hyperpolarized noble gases (HNGs) provide exciting possibilities for MR imaging at ultra-low magnetic field strengths (<0.15 T) due to the extremely high polarizations available from optical pumping. The fringe field of many superconductive magnets used in clinical MR imaging can provide a stable magnetic field for this purpose. In addition to offering the benefit of HNG MR imaging alongside conventional high field proton MRI, this approach offers the other useful advantage of providing different field strengths at different distances from the magnet. However, the extremely strong field gradients associated with the fringe field present a major challenge for imaging since impractically high active shim currents would be required to achieve the necessary homogeneity. In this work, a simple passive shimming method based on the placement of a small number of ferromagnetic pieces is proposed to reduce the fringe field inhomogeneities to a level that can be corrected using standard active shims. The method explicitly takes into account the strong variations of the field over the volume of the ferromagnetic pieces used to shim. The method is used to obtain spectra in the fringe field of a high-field (1.89 T) superconducting magnet from hyperpolarized ^{129}Xe gas samples at two different ultra-low field strengths (8.5 and 17 mT). The linewidths of spectra measured from imaging phantoms (30 Hz) indicate a homogeneity sufficient for MRI of the rat lung.

Keywords: Passive shimming; Fringe field MRI; Hyperpolarized noble gas; Low-field MRI; Field inhomogeneity correction

1. Introduction

The magnetic field outside the bore of conventional superconducting magnets used in magnetic resonance (MR) imaging systems potentially provides an inexpensive and extremely stable magnetic field for imaging. While the very low field strengths available in the fringe field generally prohibits its use for most standard MR imaging applications, it may be suitable for hyperpolarized noble gas (HNG) MR imaging (^{129}Xe and ^{3}He). This is because, unlike conventional proton MR imaging where the signal-to-noise ratio (SNR) strongly depends on the field strength, the SNR of HNG MR imaging is less dependent on the field strength and more dependent on the laser polarization conditions, such as laser power and gas mixture [1,2].

MR imaging at ultra-low magnetic field strengths (<0.15 T) also reduces the effects of chemical shift and susceptibility differences in heterogeneous samples [3], resulting in reduced image distortion and artifacts while increasing the apparent transverse relaxation time, T_2^*, and improving the spectral bandwidth. Low-field imaging may also reduce considerably the cost of the MR imaging systems since less expensive magnets can be used and less powerful RF transmitter and gradient power supplies are required. Low field imaging also

* Corresponding author. Fax: +1 519 663 3900.
E-mail address: jprobles@imaging.robarts.ca (J. Parra-Robles).

1090-7807/$ - see front matter © 2005 Elsevier Inc. All rights reserved.
doi:10.1016/j.jmr.2005.01.016

requires less site restrictions and provides advantages for patient accessibility, which could be attractive for applications such as interventional MR imaging [4,5].

Since the first demonstration of HNG gas MR imaging of excised mouse lungs by Albert et al. [6] there have been numerous advances in the use of ultra-low magnetic fields for both hyperpolarized ^{3}He (helium) and hyperpolarized ^{129}Xe (xenon) imaging. Saam et al. [7] obtained 1D profiles of helium gas samples at 3.1 mT. Darrasse et al. [8] demonstrated human helium lung imaging at 0.1 T. Augustine et al. [9] imaged helium and solid xenon at liquid helium temperatures (4 K) and 54 μT using superconductive quantum interference devices (SQUID). Tseng, Wong, and co-workers obtained 2D images at 2.1 mT from helium in sealed glass phantoms [10] and excised rat lungs [11]. More recently, Wong-Foy et al. [12] used SQUID to obtain images of xenon in porous materials at 2.3 mT. All these previous studies were performed within the bore of dedicated magnets, usually resistive.

The possibility of exploiting the fringe field available from a superconducting magnet has been explored previously for diffusion experiments [13,14] by taking advantage of the very large (typically 20–100 mT/m) field gradients present near the magnet. However, these extremely strong field gradients while useful for measurement of diffusion, pose a major obstacle for imaging applications where high homogeneity is required. Correction of these gradients using standard active shimming techniques (field correction using resistive coils) would require impractically high shim currents. Even if such high power shim supplies were available they would be expensive, and limited by temporal stability and heating concerns.

An imaging method that does not correct for the field gradient but instead uses it for spatial encoding has been proposed [15]. Although this is an attractive alternative, it does have limitations due to the presence of a strong gradient during excitation pulses, which limits it to very thin slices, significantly reducing the achievable SNR. This fact also prohibits the use of 3D imaging techniques, limits the slice orientation and requires very short echo times (TE). Furthermore, for very low Larmor frequencies, the available bandwidth is governed by the RF coil, which further limits the inhomogeneity that can be tolerated. For these reasons, it is desirable to correct the fringe field as much as possible using passive shimming, provided by the placement of ferromagnetic pieces.

In commonly used passive shimming techniques inside the magnet [16,17], it is generally assumed that the field over the volume of the ferromagnetic pieces is constant. Furthermore, it is assumed that ferromagnetic pieces located at the same radial distance from the magnet's centre but at different angular positions will experience the same field (i.e., cylindrical symmetry). This is the basis of standard passive shim design and permits the production of relatively pure field harmonics. While these assumptions are generally true in the relatively homogeneous and symmetric field near the centre of a solenoidal superconducting magnet, they are not valid for the fringe field.

In this work, a simple passive shimming method is described theoretically and used to reduce the fringe field inhomogeneities of a 1.89 T superconducting magnet to a level correctable with standard active shims. The proposed method explicitly takes into account the strong variations of the fringe field strength over the volume of the ferromagnetic pieces and the lack of cylindrical symmetry of the field about the centre of the volume of interest (VOI). This approach makes it straightforward to shim the fringe field at different distances from the superconductive magnet. In the implementation described, two different sets of steel rods parallel to the z-axis (i.e., superconducting magnet axis) and at different distances from the magnet isocentre are used to correct the magnetic field within two different volumes (2 and 6 cm diameter spheres) at field strengths (8.5 and 17 mT, respectively). The implications of this passive shimming procedure for HNG imaging of the rat lung are discussed.

2. Theory

The scalar potential at point $P(\vec{r})$ (Fig. 1) produced by an infinitesimal volume $\mathrm{d}V$ of shim element, of susceptibility χ, located at position $Q(\vec{r}')$ is given by [16,17]

$$\mathrm{d}\Phi = \frac{-\chi H_z(\vec{r}')}{4\pi}\hat{k}\cdot\nabla_Q\left(\frac{1}{|\vec{r}-\vec{r}'|}\right), \tag{1}$$

where $\hat{k}$ is the unit vector in the z direction, $\vec{r}$ and $\vec{r}'$ are position vectors for points P and Q, respectively, and ∇_Q is the gradient with respect to Q. To obtain the total

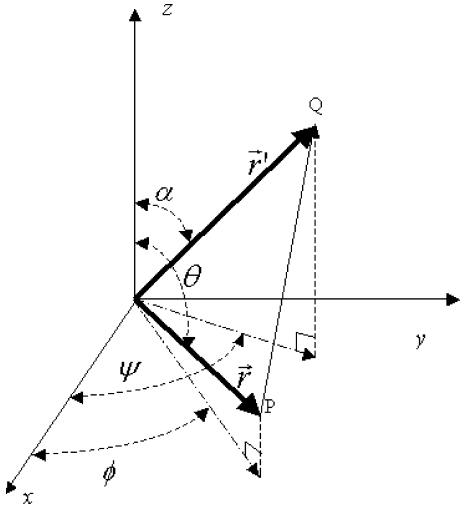

Fig. 1. Coordinate system for calculation of the magnetic field at point P arising from a point element of susceptibility χ located at point Q.

potential Φ, in the presence of a shim element, this equation must be integrated over the volume of the element V_{elem} giving:

$$\Phi = \frac{-\chi}{4\pi} \int_{V_{\text{elem}}} \mathrm{d}V \; \mathrm{H}_z(\vec{r}\,') \frac{\partial}{\partial z'} \left(\frac{1}{|\vec{r} - \vec{r}\,'|} \right). \tag{2}$$

Taking into account that $H = -\nabla_P \Phi$ and changing the order of the derivative and integral operations, the magnetic field in the z direction is given by:

$$H_z(\vec{r}) = \frac{-\chi}{4\pi} \int_{V_{\text{elem}}} \mathrm{d}V \; H_z(\vec{r}\,') \frac{\partial}{\partial z'} \frac{\partial}{\partial z} \left(\frac{1}{|\vec{r} - \vec{r}\,'|} \right). \tag{3}$$

Expanding $1/|\vec{r} - \vec{r}\,'|$ in spherical harmonics [16,17] as:

$$\frac{1}{|\vec{r} - \vec{r}\,'|} = \sum_{n=0}^{\infty} \sum_{m=0}^{n} \varepsilon_m \frac{(n-m)!}{(n+m)!} P_{n,m}(\cos\alpha) \times \frac{r^n}{f^{n+1}} P_{n,m}(\cos\theta) \cos\left[m(\phi - \psi)\right], \tag{4}$$

where $P_{n,m}$ are the associate Legendre functions of order n and degree m; $\varepsilon_m = 1$ for $m = 0$ and $\varepsilon_m = 2$ for $m \neq 0$. Using the properties of spherical harmonics to find the derivatives in Eq. (3) and taking the sums out of the integral, the following expression can be obtained:

$$H_z(r,\theta,\phi) = -\frac{1}{4\pi} \sum_{n=0}^{\infty} \sum_{m=0}^{n} A_{n,m} r^n P_{n,m}(\cos\theta) \times \left[\cos m\phi H_{n,m} + \sin m\phi K_{n,m}\right], \tag{5}$$

where

$$A_{n,m} = -\varepsilon_m \frac{(n-m+2)!}{(n+m)!},$$

$$H_{n,m} = \chi \int_{V_{\text{elem}}} \frac{H_z(\vec{r}\,')}{f^{n+3}} P_{n+2,m}(\cos\alpha) \cos m\psi \; \mathrm{d}V, \tag{6.1}$$

$$K_{n,m} = \chi \int_{V_{\text{elem}}} \frac{H_z(\vec{r}\,')}{f^{n+3}} P_{n+2,m}(\cos\alpha) \sin m\psi \; \mathrm{d}V. \tag{6.2}$$

If more than one shim element is used, the principle of superposition applies and for the general case where the shim elements have different magnetic susceptibilities, the expression for the field coefficients $H_{n,m}$ and $K_{n,m}$ can be written as:

$$H_{n,m} = \sum_k H^k_{n,m}, \tag{7.1}$$

$$K_{n,m} = \sum_k K^k_{n,m}, \tag{7.2}$$

where $H^k_{n,m}$ and $K^k_{n,m}$ are the coefficients corresponding to the kth shim element of susceptibility χ_k, calculated using Eqs. (6.1) and (6.2).

For shimming within the bore of the magnet, where the field is relatively constant over the volume of the shim elements, $H_z(\vec{r}\,')$ is taken out of the integrals in Eqs. (6.1) and (6.2). However, for shimming in the fringe field, these integrals must be numerically computed from the values of the magnetic field $H_z(\vec{r}\,')$ over the volume of the shim element. Once the values of the coefficients $H_{n,m}$ and $K_{n,m}$ have been found, the field strength at every point in the volume of interest can be computed.

3. Methods

The shimming procedure was used to passively shim the fringe field at the 8.5 and 17 mT positions. The first position was located 120 cm from the centre of the superconducting magnet and was selected such that after shimming a field strength of 8.5 mT would be available over a 2 cm diameter spherical volume (DSV). The second position was selected closer to the centre of the superconductive magnet (90 cm) to obtain a field strength of 17 mT (after shimming) over a 6 cm DSV. The selection of those positions was based on an initial field mapping of the fringe field (as discussed below). The second position was expected to yield higher SNR and be more useful for in vivo (i.e., animal) imaging purposes.

3.1. MR imaging and xenon polarization systems

The ultra-low field MR imaging system described here (Fig. 2A) used the fringe field of a 30 cm bore superconductive magnet (1.89 T, Magnex, Yarnton, Oxon, England) which permitted field strengths up to 20 mT at the surface of the magnet's dewar. Imaging was accomplished using a 26 cm diameter gradient and shim set (Bruker B-GS 30/C-19, Ettlingen, Germany) powered by the gradient and shim power supplies of the 1.89 T system (Techron 7700 and Resonance Research MXA-18/4V 0, respectively) and controlled by an MRRS (Surrey, UK) MR5000 console.

The electronics were based on a polarimeter design proposed by Saam and Conradi [18]. Modifications to this design included quadrature phase detection and interfacing to the MR5000 console [2]. For the experiments at 8.5 mT, a solenoidal RF coil with a bore diameter of 10 mm, length of 12 mm (560 turns of 34 AWG coated copper wire), and tuned to 100 kHz was used as a field mapping probe and for homogeneity measurements. At 17 mT, a solenoidal RF coil of similar dimensions but with only 250 turns and tuned to 200 kHz was used for field mapping. A larger RF coil was used to obtain signals for the final active shimming and homogeneity measurements over a larger volume at 17 mT. This coil was a split solenoid of diameter 4.5 cm, length 6 and 1 cm separation between the two winding sets (each 25 mm wide and made of 50 turns of 22 AWG coated copper wire).

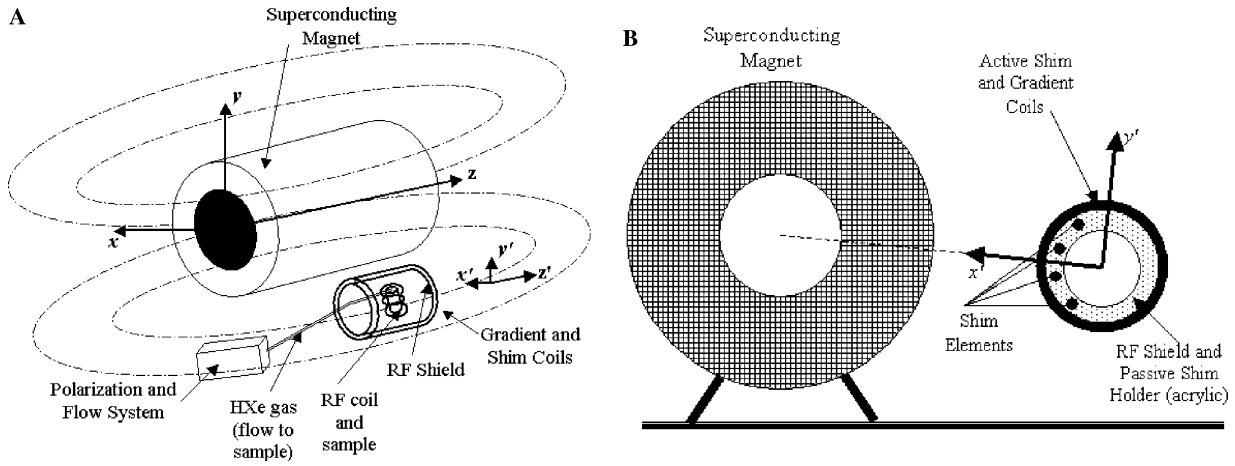

Fig. 2. (A) Schematic representation of the ultra-low field system in the fringe field of the superconducting magnet. The z'-axis is parallel to the z-axis and the origin ($z' = 0$) is aligned with the centre of the magnet ($z = 0$). (B) Transverse view of the low-field system (at right) with respect to the superconducting magnet (at left). Note the coordinates (x', y') are rotated slightly, with the x'-axis pointing in the direction of the centre of the superconducting magnet.

Hyperpolarized natural abundance xenon gas (26.4% ^{129}Xe) was produced continuously from a gas mixture (1% xenon, 10% nitrogen, and 89% helium) using a flow polarization system described previously [2,19]. The system used circularly polarized light from a 60 W diode array laser ($\lambda = 794.8$ nm, Coherent, Santa Clara, USA) and produced xenon polarizations of up to 20% at a gas flow rate of 3.5 cc/min (at room temperature and 1 atm pressure).

3.2. Shimming method

The gradient/shim coil set was positioned with its axis (z') parallel to the magnet's axis (i.e., aligned with the magnetic field direction) and slightly lower along the y-axis (Fig. 2B) due to space restrictions in the magnet room, which were imposed by the presence of the xenon polarization system and walls. Also due to these restrictions the two positions were located on different sides of the magnet (right for 8.5 mT and left for 17 mT).

The gradient/shim set was rotated about this axis by an angle such that the x' direction of the gradient/shim set pointed towards the magnet centre as shown in Fig. 2B. This choice of geometry simplified the calculations by making the field variations symmetric about the x'-axis. The acrylic end pieces located between the two layers of the RF shield served to hold the shimming elements (Fig. 2B).

Initial field mapping was performed using a Hall-effect gaussmeter (FW Bell 640, Orlando, FL, USA) and a simple probe positioning system consisting of a circular piece of acrylic, containing an array of precision holes in the $x'y'$ plane to accommodate the probe, that could be moved along the axis of the gradient/shim set to different z' positions. Once the field was passively shimmed (as described below) to a level that permitted xenon signals to be observed directly, field mapping was performed more rigorously using continuously flowing xenon gas through the RF coil which was moved to different positions within the gradient/shim set and enabled precision field mapping in a relatively short time (1–2 min per measurement point).

Commonly available construction steel rods of diameters ranging between 1 and 3 cm were used as shim elements (Fig. 3). As a first step, the magnetic susceptibility χ of the steel was experimentally measured by mapping of the effect of one pair of steel rods on the fringe field and comparing the generated spatial field harmonics to those predicted for equivalent steel rods of similar

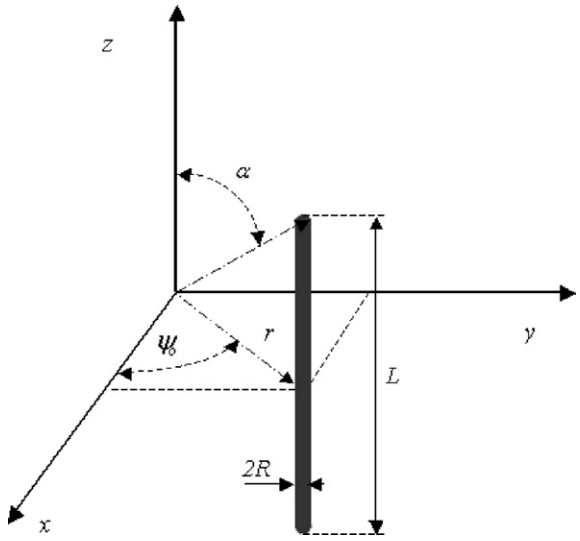

Fig. 3. Diagram of the positioning of a rod parallel to the z-axis and symmetric about the xy plane with centre at (r_0,α_0,ψ_0) and length $L = 2r_0/\tan\alpha$. In the practical implementation, the z-axis is directed horizontally and parallel to the superconducting magnet's axis.

dimensions and susceptibility equal to one. The initial estimate for the shim set parameters was obtained by assuming the field strength to be constant over the volume that would be occupied by the rod and using the standard passive shimming calculation technique [16,17]. The number of steel rods needed to produce the desired correction of the field gradient depended on the lowest order harmonic introduced that would be tolerated for the desired target field homogeneity. This order is usually determined by the size of the desired volume of homogeneity [16,17]. However, for this work, this condition was relaxed to allow harmonics to be introduced up to the point where they were correctable by the corresponding active shim to use as little passive shimming material as possible.

The optimum arrangement of shim elements to produce the desired correction was obtained using an optimization procedure that iteratively adjusted the following parameters: radius R, distance from the centre r, and length L ($L = 2r/\tan\alpha$), from the initial estimate and numerically calculating $H_z(r,\theta,\phi)$ using Eqs. (5) and (6), and the measured field maps. For simplicity, the angular position ψ was not changed from the initial estimates, but could be varied as well.

This procedure was implemented using the optimization toolbox (simple search minimization algorithm) in Matlab 6.5 (The Mathworks, Natick, MA, USA) and the field coefficients to be minimized were expressed in the form:

$$\mathcal{H}_{n,m} = \sqrt{(H_{n,m})^2 + (K_{n,m})^2}. \quad (8)$$

After correcting most of the field inhomogeneities using the steel rods, the field homogeneity was improved further using the active shims, which were systematically adjusted to provide the narrowest line-shape. The linewidth was estimated by fitting the spectra to a Lorentzian function. Spectra were obtained by releasing the xenon gas (in continuous flow mode) into imaging phantoms: a 10 mm diameter open glass cell and a 3.7 cm diameter hollow plastic ball (which approximates the rat lung volume).

4. Results

For the 8.5 mT position, the shimming procedure resulted in a set of two 1.2 cm diameter steel rods with dimensions given in Table 1 and Fig. 4A. The x'-axis was rotated 54° clockwise about the z direction from the x-axis to make field variations symmetric about the x'-axis. At the 17 mT position, the optimum shim set consisted of two pairs of steel rods (Table 1 and Fig. 4B), with the x'-axis rotated 16° counterclockwise. The estimated magnetic susceptibility of the steel ranged between 10.5 and 15.7 for the 17 mT configuration and 25.4 and 27.7 for the 8.5 mT configuration.

Table 1
Dimensions of the two optimal shim sets used at 8.5 and 17 mT (fourth column)

	Parameter	Initial estimate (mm)	Optimized design (mm)
1 Pair of rods (8.5 mT)	R	6.0	6.0
	r_0	90	90
	L	220	207
2 Pairs of rods (17 mT)	R_1	8.0	8.0
	R_2	8.0	9.5
	r_1	90	90
	r_2	90	97
	L_1	300	260
	L_2	300	340

For comparison, initial estimates obtained using the standard shim calculation method are shown in the third column.

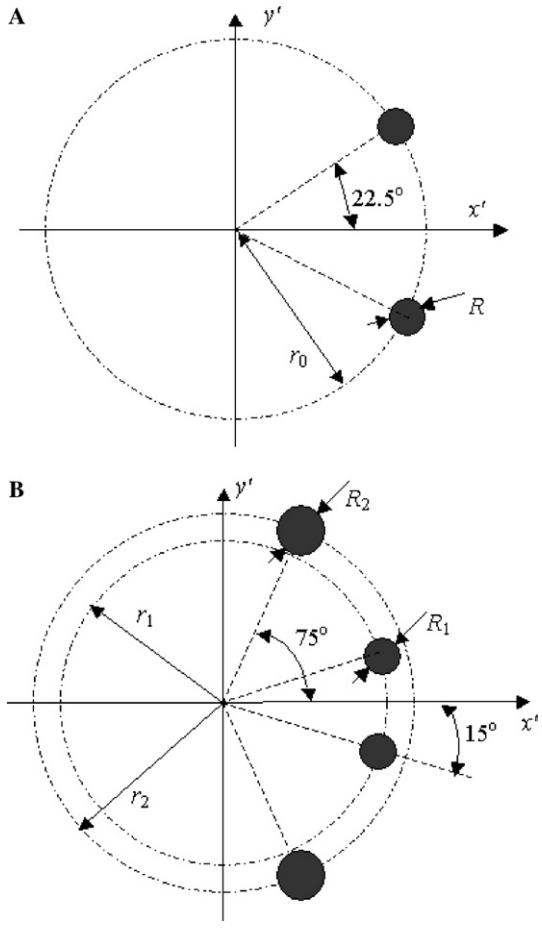

Fig. 4. Diagram ($x'y'$ plane) of the location of the steel rods used as passive shims for the two shim sets of: (A) one pair of rods at 8.5 mT and (B) two pairs of rods at 17 mT. The solid circles represent the steel rods as seen end on.

Fig. 5A shows the results of the field mapping of the fringe field along the radial direction (x') at the 8.5 mT position. A strong approximately linear gradient

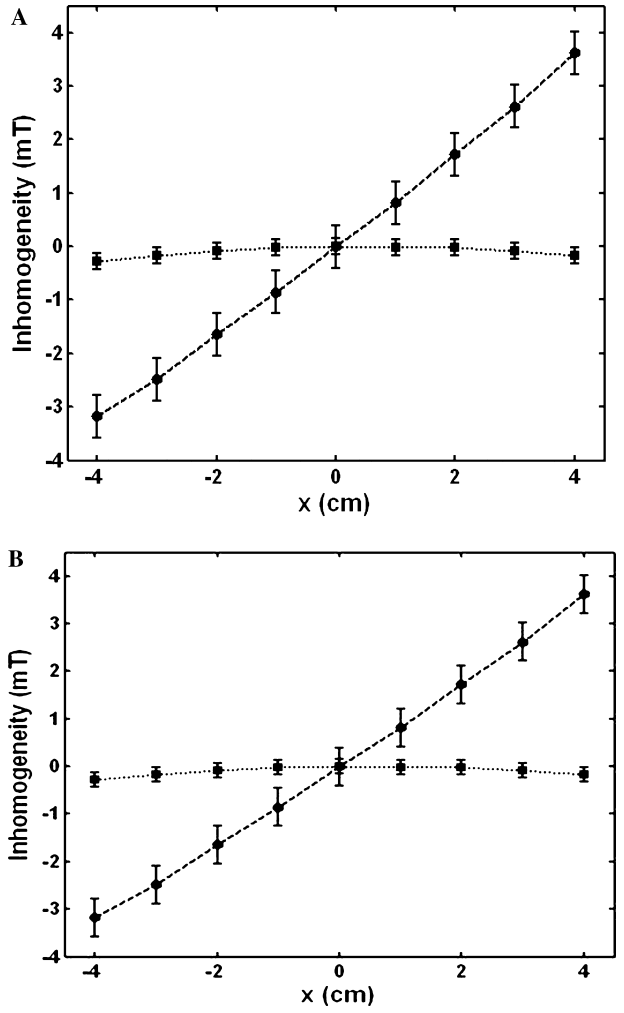

Fig. 5. Magnetic field strength plotted along the x-axis in the fringe field before (solid) and after (dotted) the passive shimming for the 8.5 mT (A) and 17 mT (B) positions. Lines are shown as an aid to the eye, only. Error bars account for instrument (gaussmeter) and positioning errors.

(30 mT/m) was found to be the main contributor to the field inhomogeneity.

The results of the field mapping at the 17 mT position are shown in Fig. 5B. At this position, a strong field gradient (92 mT/m) was found to be the main contributor to the field inhomogeneity. Figs. 5A and B also show the field maps for both positions after field correction using the passive shims.

At 8.5 mT, the strong field gradient (30 mT/m) was effectively removed using the passive shims improving the field homogeneity to 0.1% over the 2 cm DSV from the initial 7.2%.

The shim set design that produced the correction at 8.5 mT is significantly different from the initial estimate (Table 1). The rods are 1.3 cm shorter (20.7 cm). This difference is due to the relatively strong variation of the field strength over the length of the rod, mainly in the form of a second-order zonal harmonic $H_{2,0}$. As a result, the initial estimate does not minimize the $H_{2,0}$ harmonic and would have resulted in the introduction of a relatively large inhomogeneity (6.35×10^{-4} mT/cm^2). The optimized shim set produced a $H_{2,0}$ harmonic two orders of magnitude smaller (6.70×10^{-6} mT/cm^2) while producing a $H_{1,1}$ harmonic (the desired field correction) larger (-31 mT/m) than the one produced by the initial estimate design (-27 mT/m).

At 17 mT, the very strong field gradient (92 mT/m) was canceled (Fig. 5B) by the passive shims increasing the field homogeneity to 0.2% over the 6 cm DSV from the initial 25%. In this case (Fig. 4B and Table 1), due to the lack of cylindrical symmetry with respect to the centre of the volume of interest, the field strength at the positions of the two pairs of rods is different. The initial shim estimate introduces second ($H_{2,2} = 1.12 \times 10^{-2}$ mT/cm^2) and third ($H_{3,3} = 1.12 \times 10^{-2}$ mT/cm^3) order harmonics while the optimized design, by using pairs of rods with different diameters and located at different distances from the centre of the volume of interest, compensates for the field asymmetry and produces

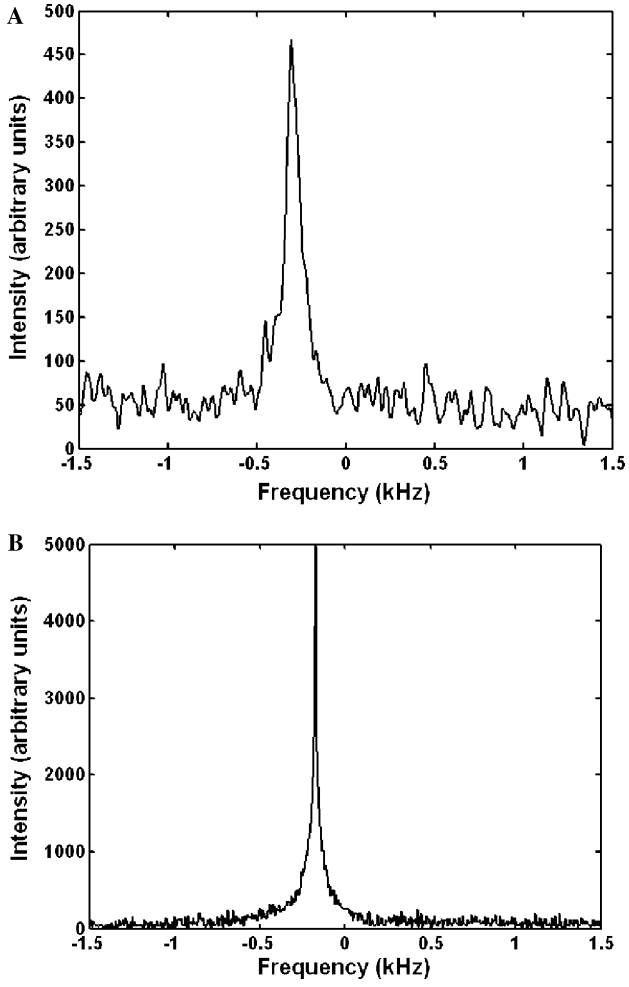

Fig. 6. Spectra obtained from a 1 cm diameter glass cell at 8.5 mT after (A) passive shimming (linewidth ~100 Hz), and (B) both passive and active shimming (linewidth ~20 Hz).

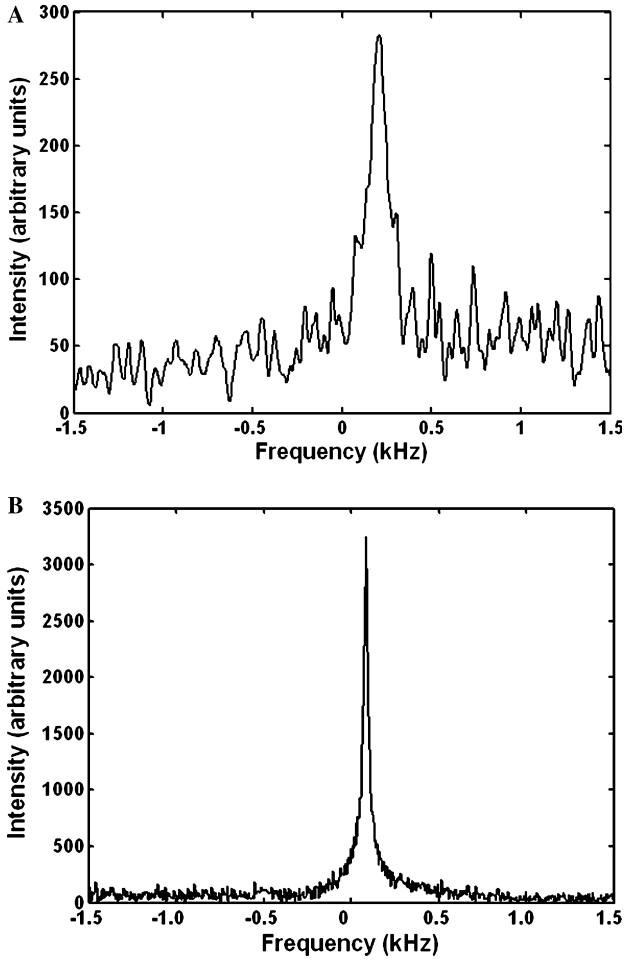

Fig. 7. Spectra obtained from a 3.7 cm diameter spherical phantom at 17 mT after (A) passive shimming (linewidth ~200 Hz), and (B) both passive and active shimming (linewidth ~30 Hz).

much smaller second ($H_{2,2} = 2.02 \times 10^{-5}$ mT/cm^2) and third ($H_{3,3} = 9.22 \times 10^{-4}$ mT/cm^3) order harmonics. Similarly to the case of one pair of rods, the new method uses shorter rods which minimizes $H_{2,0}$ and maximizes the desired $H_{1,1}$ correction.

Fig. 6A shows the xenon spectrum obtained at 8.5 mT after passive shimming (linewidth approximately 100 Hz). Fig. 6B shows the spectrum after both passive and active shimming (linewidth: ~20 Hz). Fig. 7A shows the xenon spectrum (linewidth: ~200 Hz) obtained at 17 mT after passive shimming. Fig. 7B shows the spectrum after both passive and active shimming (linewidth: ~30 Hz). The linewidth obtained are better than the target homogeneity of 40 Hz, which was desired for the imaging experiments. It should be noted that no signals were observable in either case without the passive shims.

5. Discussion

The purpose of this work was to develop a method to shim the fringe field of a superconducting magnet to produce a homogenous region for hyperpolarized gas imaging. The method extends the conventional passive shimming method [16,17] to the case of the inhomogeneous and asymmetric fringe field outside the bore of a superconducting magnet.

The practical implementation of the shimming procedure at two positions in the fringe field of the superconducting magnet produced the desired volumes of homogeneity at 8.5 mT (2 cm DSV) and 17 mT (6 cm DSV), sufficient to allow xenon signals to be obtained (Figs. 6A and 7A), thus permitting improved homogeneity by active shimming using these signals. The final field homogeneity (approximately 0.017%) allowed reasonable xenon spectra to be obtained (Figs. 6B and 7B) with a linewidth of 19 ± 3 Hz at 8.5 mT and 33 ± 6 Hz at 17 mT. The shimmed line-shape was well approximated by a Lorentzian function (hence the FWHM is a good indicator of the harmonic content of the field). Further homogeneity improvements were not possible due to the lack of fourth order zonal harmonic ($H_{4,0}$) correction in the active shim system used.

It should be noted that though the final homogeneity (0.02% or 200 ppm) seems large compared to the typical field homogeneity in clinical systems (<10 ppm), this is a relative quantity, which depends on the static magnetic field strength. For imaging purposes the homogeneity requirement is that the linewidth produced by the field inhomogeneities must be smaller than the desired pixel size (in frequency units). A homogeneity of 200 ppm at 17 mT (0.0034 mT or 40 Hz for ^{129}Xe) is comparable to a homogeneity of 1.5 ppm at 1.89 T (0.0030 mT or 35 Hz for ^{129}Xe), which is quite acceptable.

Though the differences between the optimized shim sets and the initial estimates can be as small as a few millimeters, they strongly affect the field correction produced by the shim sets, resulting in differences of several orders of magnitude. Consequently, the shim sets have to be accurately constructed. It would be preferable to construct a shim holder that would allow for fine positioning (accurate to within 0.1–0.5 mm) of the shimming elements. As well, this is just one approach to optimizing the shim set design and others are possible including varying χ and/or ψ.

One limitation of this shimming method is that it assumes the fringe field is totally in the z direction. This is probably a good assumption if the volume of interest is not too large and is selected close to the superconducting magnet and in line with its isocentre, where the field lines are approximately parallel to the z-axis.

The presence of the steel rods in the fringe field did not greatly affect the homogeneity inside the superconducting magnet. The largest estimated field inhomogeneity introduced was about 5 ppm, which is easily correctable by the active shims of the high-field system. The forces exerted on the steel rods by the magnetic field were small enough that no anchoring for the system was

needed. At higher fields or when using larger amounts of steel, this factor may require careful consideration.

This method is not restricted to the use of steel as the shimming material and an attractive alternative is the use of permanent magnets as shimming elements. In this way, higher field strengths may be obtained. Combining steel and permanent magnets could also provide very useful shim designs with improved correction symmetry.

The estimated susceptibilities seem to be lower than those found in the literature [20] for most soft steels. It should be noted that all the rods are located in regions where the original field strength is much larger (typically 2–3 times) than the final strength obtained at the centre of the homogeneous region. However, since the exact composition of the steel used in this work was unknown, no proper comparison to reported values can be made. Other effects such as the fact that the field strength strongly varies over the region occupied by the rods and possible hysteresis effects can also have influenced the obtained susceptibility estimates. Furthermore, the susceptibility values estimated in this work show a relatively large variation. This can be explained by the fact that each pair of rods is located at positions with substantially different field strengths.

This approach makes it straightforward to shim the fringe field at different distances from the superconductive magnet. In this way, it is possible to perform MR imaging experiments at several field strengths using a single superconducting MR magnet, which may be very useful to study the field strength dependence of MR parameters.

The possibility of using the fringe field of superconducting magnets (passively shimmed) for human imaging will depend on the strength of the available fringe fields and the minimum requirements for field strengths from the SNR point of view. Since many of the superconducting magnets commercially available are self-shielded (i.e., their fringe field strengths are already minimized for siting concerns) the available field strength after passive shimming over the necessary volume will likely be insufficient for human imaging. However, the introduction of higher field strengths in MR imaging (3–7 T) could provide stronger fringe fields that will make human imaging feasible. Other possibilities include the use of magnets especially designed to provide a desirable fringe field and the above discussed passive shimming with permanent magnets.

The simplicity of the method and the possibility of using most of the hardware of the high-field system to power and control the low-field system make this approach an inexpensive and a convenient way of expanding the low field capabilities of existing or new MR facilities, not only for HNG imaging but also for other techniques such as electron-spin resonance (ESR), prepolarized MR imaging (PMRI), and dynamic nuclear polarization (DNP) that may also be optimal at low magnetic field strengths. One of the most promising uses of this fringe field approach may be in dedicated low-field animal systems.

6. Conclusion

The method for passively shimming the fringe field of a MRI superconductive magnet presented here proved to be effective and produced field corrections that permitted the use of standard active shimming procedures to further improve the field homogeneity up to the level needed to obtain MR images.

The simplicity of the method and the possibility of using most of the hardware of the high-field system to power and control the high-field system make this approach an inexpensive and a convenient way of expanding the low field capabilities of existing or new MRI facilities for HNG imaging.

Acknowledgments

The authors thank Philippe Gravelle and Ernie Neuheimer from Carleton University for their technical assistance. This project was supported by the Natural Sciences and Engineering Research Council (NSERC) of Canada and by the Ontario Centre of Excellence for Breast Cancer Imaging Research.

References

[1] J. Parra-Robles, A.R. Cross, G.E. Santyr, Theoretical magnetic field dependence of the signal-to-noise ratio and spatial resolution for hyperpolarized noble gas magnetic resonance imaging of the lungs, Med. Phys. 23 (2005) 221–229.
[2] A.R. Cross, M. McDonald, J. Parra Robles, G.E. Santyr, Laser-polarized ^{129}Xe NMR at 1.88 T and 8.5 mT: A signal-to-noise ratio comparison, J. Magn. Reson. 162 (2003) 241–249.
[3] R. Sepponen, J. Sipponen, A. Sivula, Low field (0.02 T) nuclear magnetic resonance imaging of the brain, J. Comp. Assist. Tomogr. 9 (1985) 237–241.
[4] S.K. Koskinen, R.K. Parkkola, J. Karhu, et al., Orthopedic and interventional applications at low field MRI with horizontally open configuration: A review, Der Radiologe 37 (1997) 819–824.
[5] Robert C. Krempien, Kai Schubert, Dietmar Zierhut, et al., Open low-field magnetic resonance imaging in radiation therapy treatment planning, Int. J. Radiat. Oncol. Biol. Phys. 53 (2002) 1350–1360.
[6] M.S. Albert, G.D. Cates, B. Driehuys, W. Happer, B. Saam, C.S. Springer Jr., A. Wishnia, Biological magnetic resonance imaging using laser-polarized ^{129}Xe, Nature 370 (1994) 199–201.
[7] B. Saam, N. Drukker, W. Happer, Edge enhancement observed with hyperpolarized ^{3}He, Chem. Phys. Lett. 263 (1996) 481–487.
[8] L. Darrasse, G. Guillot, P.J. Nacher, G. Tastevin, Low field single shot ^{3}He MRI in human lungs, Proc. ISMRM 6th Meeting (1998), p. 449.
[9] M.P. Augustine, A. Wong-Foy, J.L. Yarger, M. Tomaselli, A. Pines, D.M. Tom That, J. Clarke, Low field magnetic resonance

images of polarized noble gases obtained with a DC superconducting quantum interference device, Appl. Phys. Lett. 72 (1998) 1908–1910.

[10] C.H. Tseng, G.P. Wong, V.R. Pomeroy, R.W. Mair, D.P. Hinton, D. Hoffmann, R.E. Stoner, F.W. Hersman, D.G. Cory, R.L. Walsworth, Low field MRI of laser polarized noble gas, Phys. Rev. Lett. 81 (1998) 3785–3788.

[11] G.P. Wong, C.H. Tseng, V.R. Pomeroy, R.W. Mair, D.P. Hinton, D. Hoffmann, R.E. Stoner, F.W. Hersman, D.G. Cory, R.L. Walsworth, A system for low field imaging of laser-polarized noble gas, J. Magn. Reson. 141 (1999) 217–227.

[12] A. Wong-Foy, S. Saxena, A.J. Moulé, H.M.L. Bitter, J.A. Seeley, R. McDermott, J. Clarke, A. Pines, Laser polarized ^{129}Xe NMR and MRI at ultralow magnetic fields, J. Magn. Reson. 157 (2002) 235–241.

[13] R. Kimmich, W. Unrath, G. Schnur, E. Rommel, NMR measurement of small self-diffusion coefficients in the fringe field of superconducting magnets, J. Magn. Reson. 91 (1991) 136–140.

[14] D. Wu, C.S. Johnson Jr., Diffusion-ordered 2D NMR in the Fringe field of a superconducting magnet, J. Magn. Reson. A 116 (1995) 270–272.

[15] Z.H. Cho, E.K. Wong Jr., Fringe Field MRI, U.S. Patent # 5,023,554, June 11 (1991).

[16] F. Romeo, D.I. Hoult, Magnet profiling: Analysis and correcting coil design, Magn. Reson. Med. 1 (1984) 44–65.

[17] D.I. Hoult, D. Lee, Shimming a superconducting nuclear-magnetic-resonance imaging magnet with steel, Rev. Sci. Inst. 56 (1985) 131–135.

[18] B.T. Saam, M.S. Conradi, Low frequency NMR polarimeter for hyperpolarized gases, J. Magn. Reson. 134 (1998) 67–71.

[19] I.L. Moudrakovski, S. Lang, C.I. Ratcliffe, B. Simard, G. Santyr, J. Ripmeester, Chemical shift imaging with continuously flowing hyperpolarized xenon for the characterization of materials, J. Magn. Reson. 144 (2000) 372–377.

[20] American Society for Metals, Metals Handbook, ASM International Handbook Committee, Ohio (1990), p. 374.